nature geoscience

SUPPLEMENTARY INFORMATION

DOI: 10.1038/NGEO2772

Redox-induced lower mantle density contrast and effect on mantle structure and primitive oxygen

Tingting Gu, Mingming Li, Catherine McCammon and Kanani K. M. Lee

Supplementary Table 1.

Normalized chemical composition in mol% of the enstatite chondrite model of the lower mantle[12] for samples used in this study: J95_RED for a more reduced starting glass as compared to J95_OX for a more oxidized starting glass. Also shown is a standard model for mantle composition, pyrolite, for comparison[50]. Note: FeO abundance listed here includes all Fe, both ferric and ferrous.

MgO	SiO_2	Al_2O_3	CaO	FeO	(Mg+Fe)/Si	$Fe^{3+}/\Sigma Fe$	Reference
36.85	47.30	1.21	1.68	12.95	1.053	0.30 (±0.04)	This study, J95_RED
37.13	47.32	1.18	1.63	12.74	1.054	0.35 (±0.04)	This study, J95_OX
37.07	47.69	1.12	1.65	12.46	1.039	N/A	Enstatite Chondrite LM[12]
49.38	39.19	2.28	3.31	5.84	1.409	N/A	Pyrolite[50]

Supplementary Table 2.

Synthesis conditions and synthesized phases as determined by XRD and SEM for the J95_RED and J95_OX phases. Room-pressure Bm volumes and lattice parameters are listed. Values for samples that were not recovered from high pressures and thus with no direct measurement of ambient pressure volumes are indicated by N/A.

$P_{dia.}$ (GPa) [a]	$P_{Ne/Ar}$ (GPa) [b]	T (K)	Heating duration (mins)	P medium	Bm V_0 (Å^3)	Bm a_0 (Å)	Bm b_0 (Å)	Bm c_0 (Å)	Phases IDed by XRD	Phases IDed by SEM
Sample: J95_RED										
30±0.5	29.5±0.1	2000±100	23	Ne	164.83 ±0.10	4.800 (1)	4.950 (1)	6.935 (1)	Bm, St	Bm, Al_2O_3
47±0.5	46.7±0.3	2100±50	24	Ne	164.94 ±0.10	4.801 (1)	4.952 (1)	6.937 (1)	Bm, St	Bm, Al_2O_3
71±0.5	70.5±0.3	2300	17	Ne	N/A	N/A	N/A	N/A	Bm, St	N/A
88(±1)	87.8±0.5	2300	~10	Ar	165.36 ±0.10	4.804 (1)	4.958 (1)	6.943 (1)	Bm, St	Bm, Al_2O_3
Average V_0 of Bm: 165.0 (±0.4) Å^3										
Sample: J95_OX										
30±1	28.8±0.2	2000±100	>15	Ne	N/A	N/A	N/A	N/A	Bm, St	N/A
49±0.5	49±0.4	2150±50	>15	Ne	164.13±0.10	4.792 (1)	4.941 (2)	6.928 (1)	Bm, St	Bm, St
77(±2)	75±1	2350	7	Ar	164.47 ±0.10	4.794 (1)	4.949 (2)	6.933 (4)	Bm, St	Bm, St
Average V_0 of Bm: 164.3 (±0.4) Å^3										

[a] Pressure was measured according to the Raman spectroscopy of the diamond edge[38].

[b] Pressure was measured according to the diffraction lines of Ne[35] and Ar[36], all of which were located within the uncertainty range of the initial pressure measured from Raman peaks of the diamond culet[38].

Supplementary Table 3.

Chemical composition of the initial glass samples and quenched Bm based on EPMA WDS (30, 49 GPa) and EDS (88, 75 GPa) measurements of compositions (wt%). Calculations for formula and inferred $Fe^{3+}/\Sigma Fe$ ratio of Bm are explained in the Methods section of the main text. Note the larger abundance of FeO in the J95_RED samples as compared to the J95_OX samples. This accounts for most of the molar mass difference and resulting density differences between the reduced and oxidized synthesized samples. The difference in molar mass between the glass bead starting samples is minimal. Note: FeO abundance listed here includes all Fe, both ferric and ferrous. *Molar mass as oxides ($MgO \bullet FeO \bullet SiO_2 \bullet Al_2O_3 \bullet CaO$).

Sample	MgO	FeO	SiO_2	Al_2O_3	CaO	Molar mass
J95_RED, bead	27.0(2)	17.1(4)	51.9(3)	2.26(5)	1.72(2)	54.79 *
J95_OX, bead	27.3(4)	16.8(4)	52.0(5)	2.22(7)	1.67(2)	54.70 *
J95_RED, 30 GPa, Bm	27.4(4)	18.5(1)	50.3(3)	2.14(1)	1.67(1)	110.4(1)
J95_OX, 49 GPa, Bm	26.1(1)	16.8(2)	53.2(2)	2.25(1)	1.57(1)	108.3(1)
J95_RED, 88 GPa, Bm	27.5(6)	18.3(6)	50.2(5)	2.29(5)	1.64(6)	110.2(3)
J95_OX, 75 GPa, Bm	26.2(7)	16.3(8)	53.4(7)	2.24(6)	1.99(6)	108.1(4)
			Formula			**$Fe^{3+}/\Sigma Fe$**
J95_RED, 30 GPa, Bm			$Mg_{0.747}Fe^{2+}_{0.226}Fe^{3+}_{0.023}Ca_{0.033}Si_{0.920}Al_{0.046}Fe^{3+}_{0.034}O_3$			0.20(5)
J95_OX, 49 GPa, Bm			$Mg_{0.697}Fe^{2+}_{0.163}Fe^{3+}_{0.090}Ca_{0.030}Si_{0.952}Al_{0.048}O_3$			0.36(10)
J95_RED, 88 GPa, Bm			$Mg_{0.749}Fe^{2+}_{0.224}Fe^{3+}_{0.024}Ca_{0.032}Si_{0.918}Al_{0.049}Fe^{3+}_{0.032}O_3$			0.20(10)
J95_OX, 75 GPa, Bm			$Mg_{0.697}Fe^{2+}_{0.153}Fe^{3+}_{0.090}Ca_{0.038}Si_{0.953}Al_{0.047}O_3$			0.37(15)

Supplementary Table 4.

Birch-Murnaghan equation of state parameters for bridgmanite, alumina, and stishovite. Values with * were held constant and V_0 is based on values listed in Supplementary Table 2. Data for $MgSiO_3$ are from Ref.[14].

Sample	V_0 **(Å^3)**	K_0 **(GPa)**	K_0**'**	**Source**
J95_RED	165.0* (0.4)	235 (2)	4.5 (0.1)	This study
J95_RED	165.0* (0.4)	245 (1)	4*	This study
J95_OX	164.3* (0.4)	227 (2)	4.6 (0.1)	This study
J95_OX	164.3* (0.4)	240.9(0.6)	4*	This study
$MgSiO_3$	162.36(4)*	251 (2)	4.11 (7)	Ref. 14
Al_2O_3	253.7	253.0	4.3	Ref. 51
SiO_2	46.58	314.0	3.8	Ref. 51

Supplementary Figures

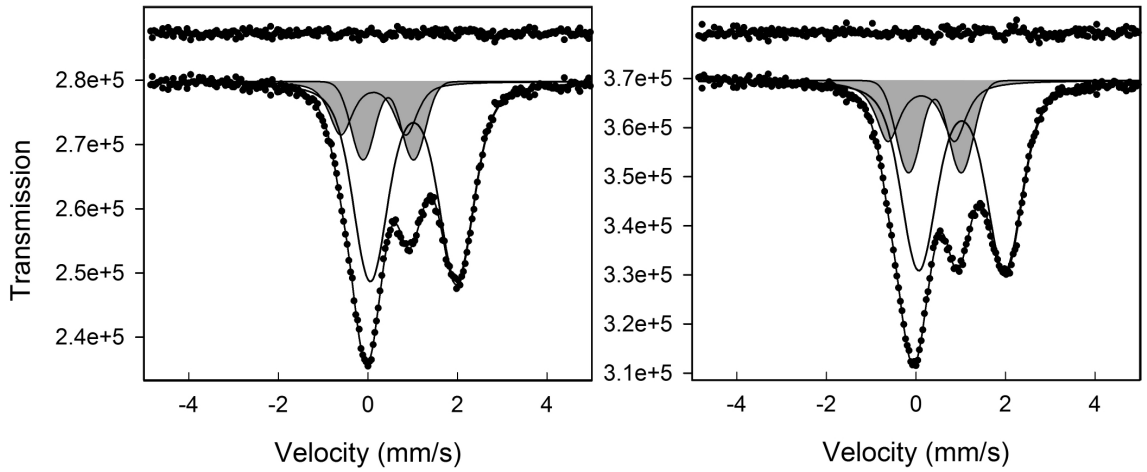

Supplementary Fig. 1. Room-temperature Mössbauer spectra of starting glass compositions. left, J95_RED and **right,** J95_OX. $Fe^{3+}/\Sigma Fe$ was determined from the relative areas with uncertainties based on multiple fitting trials using the program MossA[52] assessed with respect to χ^2, realistic values of hyperfine parameters and consistency across spectra collected using different sources. The final fit is a two-dimensional Gaussian distribution for Fe^{2+} (unshaded) and two pseudo-Voigt doublets for Fe^{3+} (grey), where the latter may indicate more than one Fe^{3+} coordination environment. The residual is shown above each spectrum.

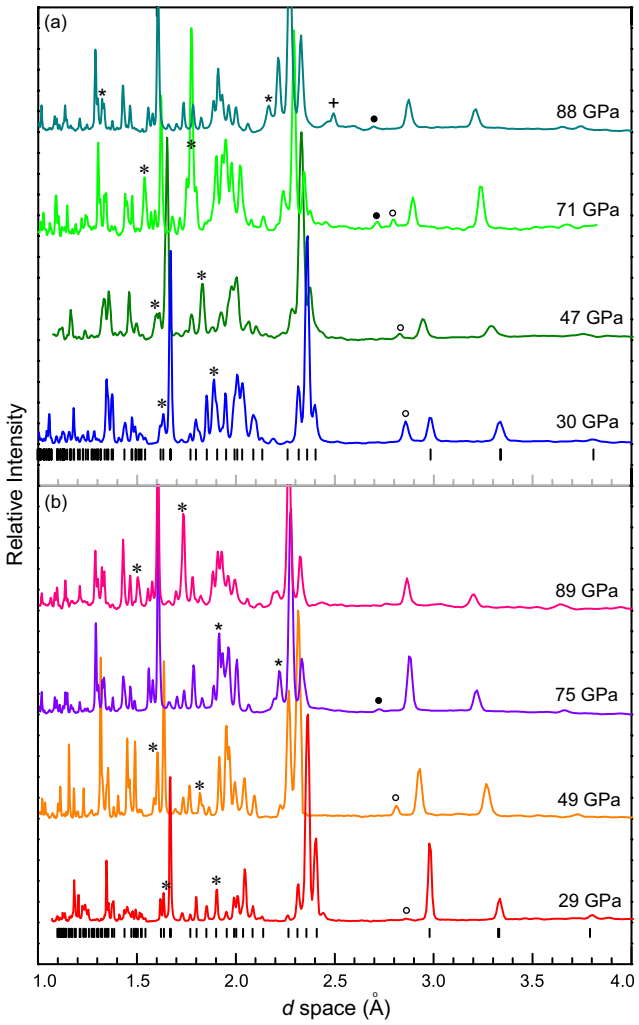

Supplementary Fig. 2. Selected XRD patterns for synthesized samples collected at room temperature. a, XRD patterns of sample J95_RED; **b,** XRD patterns of sample J95_OX. Perovskite: bars; SiO_2: (Stv) open circles, ($CaCl_2$ structure) solid circles; Ne: asterisks; Ar: stars; unidentified, possibly ppv, doublet: plus.

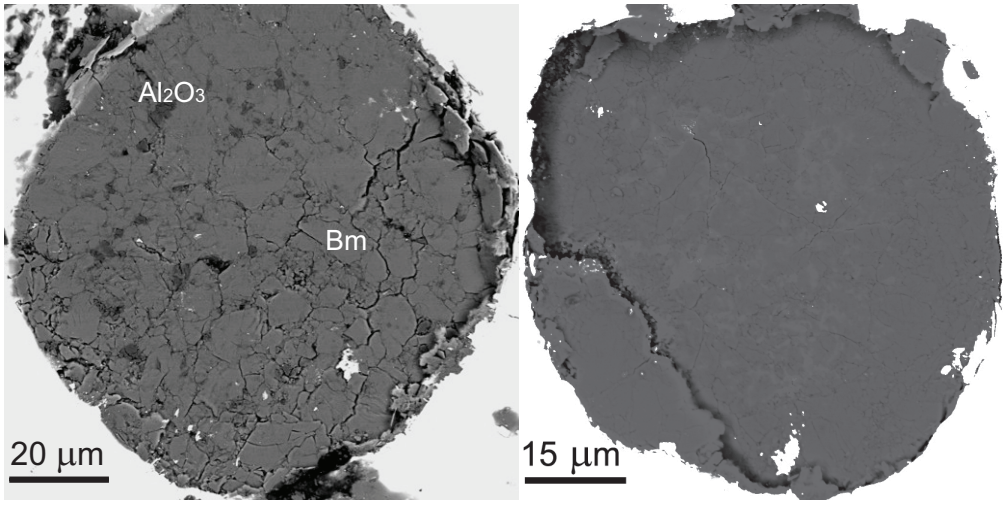

Supplementary Fig. 3. SEM images of recovered samples. left, J95_RED sample synthesized at 88 GPa. Darker grains are Al_2O_3. **right,** J95_OX sample synthesized at 49 GPa, quenched from 70 GPa. Note the lack of dark grains in the J95_OX samples, suggesting that there is no separate Al_2O_3 phase.

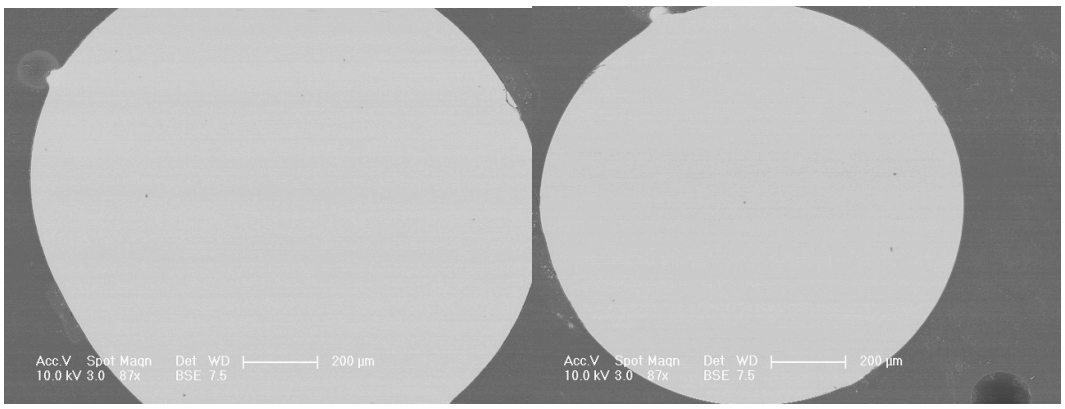

Supplementary Fig. 4. SEM images of cross-sections of the glass bead starting compositions. left, J95_RED; **right,** J95_OX. Note the homogeneous texture and color indicative of homogeneous composition.

References

50. McDonough, W. F. & Sun, S. S. The composition of the Earth. *Chemical Geology* **120**, 223–253 (1995).

51. Stixrude, L. & Lithgow-Bertelloni, C. Thermodynamics of mantle minerals - II. Phase equilibria. *Geophysical Journal International* **184,** 1180–1213 (2011).

52. Prescher, C., McCammon, C. & Dubrovinsky, L. MössA - a program for analyzing energy-domain Mössbauer spectra from conventional and synchrotron sources. *Journal of Applied Crystallography* **45,** 329-331 (2012).